Fabrication of mode-coupling-receiver chip for lossless optical splitters by femtosecond laser

QING TAO[a,b,c], JUE WANG[a,b], CHEN HU[a,b], BOWEN LU[a,b], ZHONGSHENG ZHAI[a,b,c], JIAN CHENG[a,b], DUN LIU[a,b,*]
[a]*Hubei Key Lab of Manufacture Quality Engineering, Wuhan 430068, China*
[b]*School of Mechanical Engineering, Hubei University of Technology, Wuhan 430068, China*
[c]*Hubei Key Laboratory of Modern Manufacturing Quantity Engineering, School of Mechanical Engineering, Hubei University of Technology, Wuhan 430068, Hubei, P.R. China*

In this paper, ten 8×1 mode coupling receiver chips are designed and manufactured for lossless optical splitters. The width of input ridge waveguide is 12.25 μm. Spacing between input ridge waveguides is 15.06 μm. The width of input port of tapered ridge waveguide is 210.01 μm. The length of tapered ridge waveguide is 300.41 μm. The width of output multimode ridge waveguide is 50.91 μm. The height of input ridge waveguide is 22.60 μm. The distance between straight waveguide and edge of the multimode tapered waveguide is 4.86 μm. Manufacturing error values are within the design error range. Test results show that average insertion loss≤13 dB, average return loss ≥50 dB, average directivity>55 dB. Average bit error rate is 1.583×10^{-10} in signal upstream for every input port. It is very beneficial for next-generation PONs.

(Received July 17, 2018; accepted February 12, 2019)

Keywords: Mode coupling receiver chip, Lossless splitter, PON

1. Introduction

Mode coupling receiver is an important optical component in the next generation of passive optical networks. There are two traditional mode coupled receivers for lossless optical splitter [1-2]: fused single mode fiber to multimode fiber coupler and free space lens coupler. But, they are all large in size, which is not conducive to integration for planar lightwave circuit (PLC). Therefore, we propose to design and manufacture an optical waveguide MCR chip.

Another, there are also many ways to fabricate optical waveguide chips. The laser ablation process is simple and the processing precision is high. However, the edge roughness of waveguide is large and there is ablation residue [3-4]. Ultra-violet direct writing enables large-scale processing, but production cycle is long and the etching requires strict control of photosensitive material [5-6]. Two-photon direct writing can etch the waveguide directly inside the material, but waveguide topography is not easy to control [7-8]. The proton beam direct writing can also directly engrave the optical waveguide on the material, but the processing area is limited and the forming waveguide structure is greatly affected by interface effect [9-10]. Electron beam direct writing can also etch the optical waveguide on the material, but the roughness of the optical waveguide is difficult to control [11-12]. Compared with traditional optical waveguide fabrication technology, the femtosecond laser writing technology has advantages of simple operation and high processing precision [13-14].

So, we will propose a new technique of silica-based 8×1 mode coupling receiver chip (MCRC) for lossless optical splitter by femtosecond laser writing. Experimental results are very beneficial for next-generation PONs.

2. Design of MCRC for Lossless Optical Splitter

Length, width, thickness of tapered waveguide are designed for tapered waveguide and width, distance, depth and other parameters of straight waveguide are designed for MCRC. The length of single-mode ridge waveguide is 5000 μm. The input optical wavelength is 1310±50 nm. The cladding refractive index for MCRC is 1, refractive index difference between core and cladding for MCRC is 0.4444.

There is an 1×8 lossless optical splitter in Fig. 1. In the direction of signal downstream, optical line terminal (OLT) emits signal light with the wavelength of 1490±10 nm. Signal light passes through the single-mode fiber, optical amplifier, 1×8 optical splitter and wavelength division multiplexers (WDM), finally arrives at optical network units (ONU).

In the direction of signal upstream, ONUs emits signal light with the wavelength of 1310±50 nm. Signal light goes through single-mode fiber, WDM, fiber array chip, tapered waveguide array chip, 8×1MCR chip, optical amplifier and multimode fiber, last reaches to OLT.

Because the optical amplifier compensates for the loss of the upstream and downstream optical paths, there is no loss in the overall optical paths.

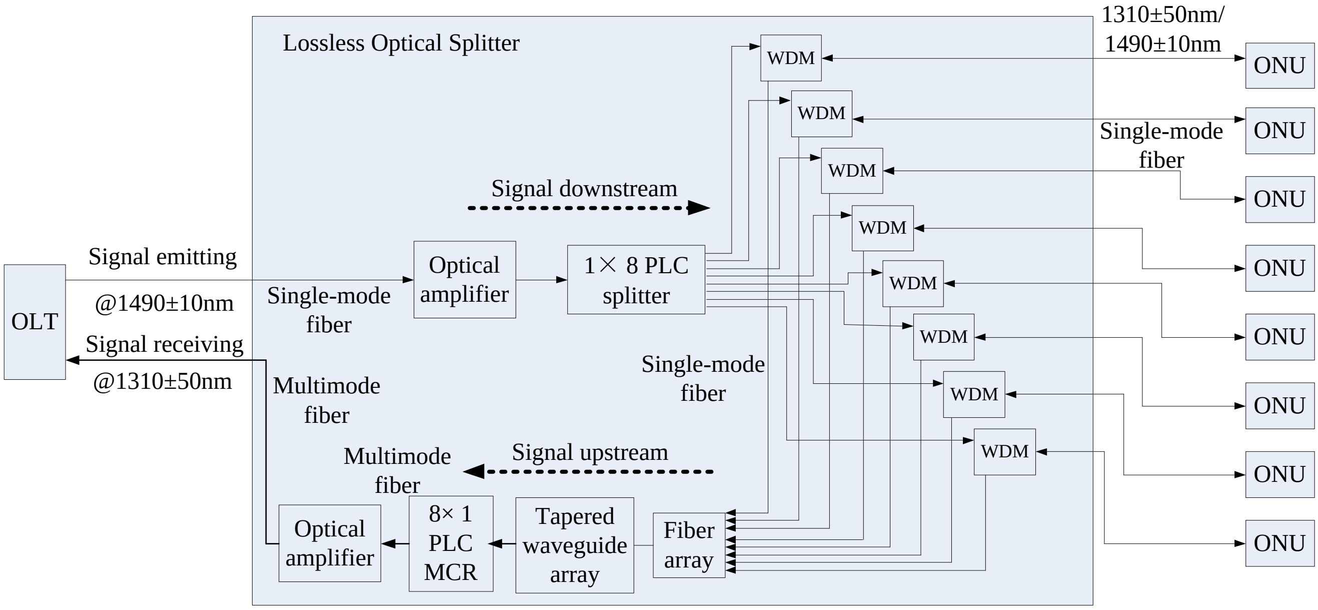

Fig. 1. System diagram of lossless splitter

MCRC is an important optical device in the lossless splitter [15-18]. The 8×1 MCRC is designed in Fig. 2. The core diameter of multimode fiber is 50 μm, the length of multimode fiber is 2 m. The distance between core edge of multimode tapered waveguide and diameter edge of multimode fiber is ***d*** μm. Refractive index of curing adhesive is 1.462@1310±50 nm. Length of the core of multimode tapered waveguide is ***α*** μm. The width of the core of single-mode ridge waveguide is ***b*** μm. The change of etching depth in single-mode ridge waveguide is ***i*** μm. The thickness of silica material is 200 μm. The distance between straight waveguides is ***c*** μm. The distance between straight waveguide and edge of the multimode tapered waveguide is 5 μm. The center wavelength of optical signal is 1310 nm. Refractive index of silica is 1.4444@1310 nm, refractive index difference between core and air cladding is 0.4444@1310 nm.

Fig. 2 (a) and Fig. 2 (b) are top view and front view of 8×1 MCRC, respectively. Fig. 2 (c) is mode field diagram of single mode ridge waveguide. In Fig. 2, there are five parameter variables: ***α, b, c, d, i***. By simulation, we can obtain the best parameter value of ***α, b, c, d, i***.

In Fig. 2(a), because input ports 5,6,7,8 are symmetry with input ports 1,2,3,4, we only calculate port 1,2,3,4 respectively. By simulation, when normalized light inputs from ports 1,2,3,4, we can obtain normalized output power and find best parameter ***α*** and ***d***.

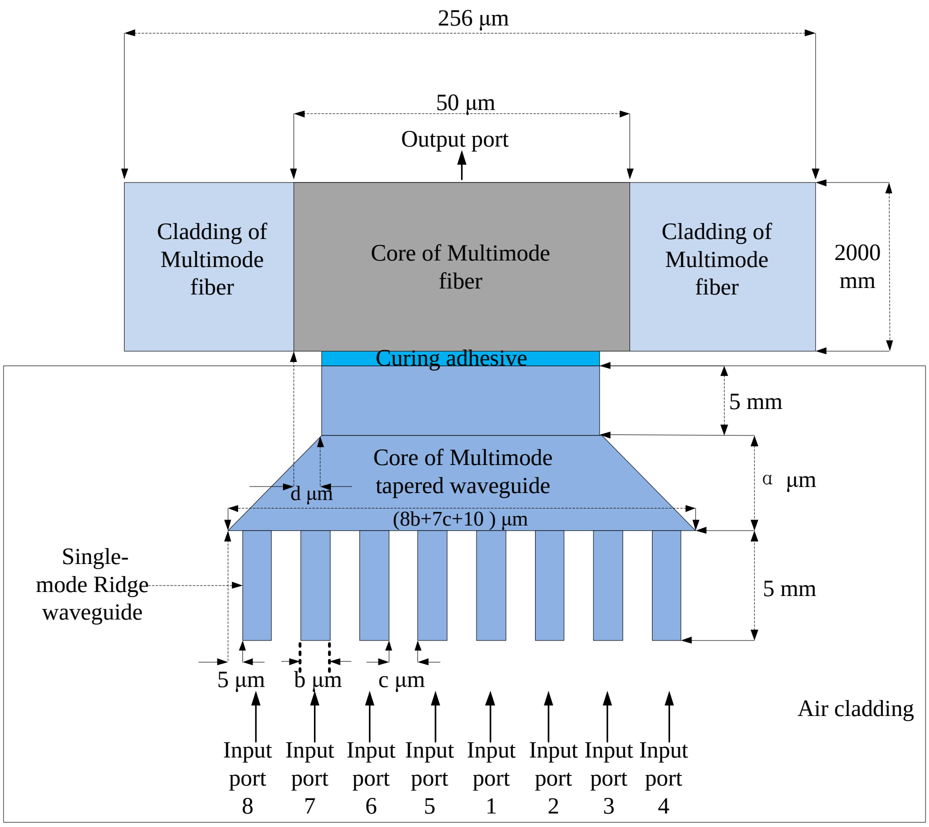

(a) Top view of MCRC design

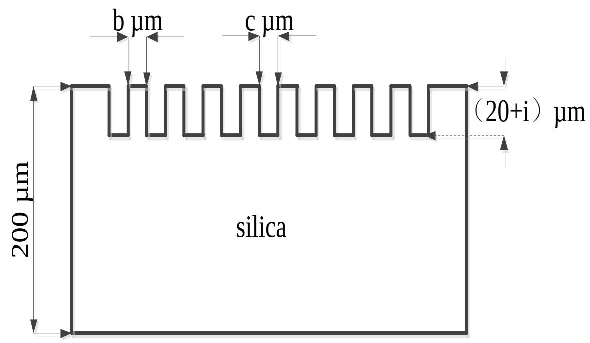

(b) Front view of input ports by simulation

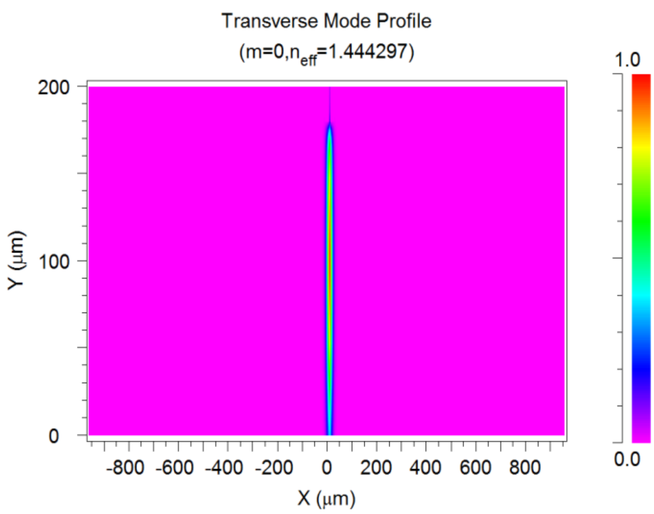

(c) Light field distribution of input port by simulation

Fig. 2. Design diagram of 8×1 MCRC

In Fig. 3(a), when light inputs from port 1, parameter ***α*** ranges from 0 to 300 μm and parameter ***d*** changes from -10 μm to 10 μm, normalized output power is greater than 0.22. In Fig. 3(b), when light inputs from port 2, parameter ***α*** ranges from 0 to 300 μm and parameter ***d*** changes from -10 μm to 10 μm, normalized output power is also greater than 0.21. In Fig. 3(c), when light inputs from port 3, parameter ***α*** ranges from 0 to 350 μm and parameter ***d*** changes from -10 μm to 10 μm, normalized output power is greater than 0.18. In Fig. 3(d), when light inputs from port 4, parameter ***α*** ranges from 0 to 700 μm and parameter ***d*** changes from -10 μm to 10 μm, normalized output power is also greater than 0.14. Summarizing the contents of above four figures, we can draw a conclusion, when parameter ***α*** changes within 0~300 μm and parameter ***d*** changes within -10 μm to 10 μm, ***α*** is the main factor of output power change. So, we set ***α***=300 μm and ***d***=0 μm.

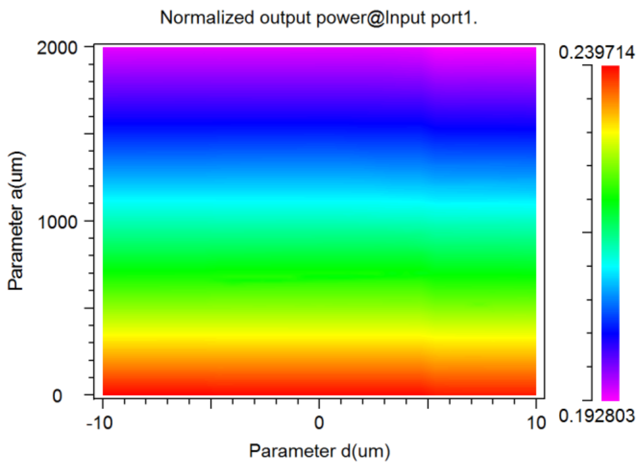

(a) Light input from port 1

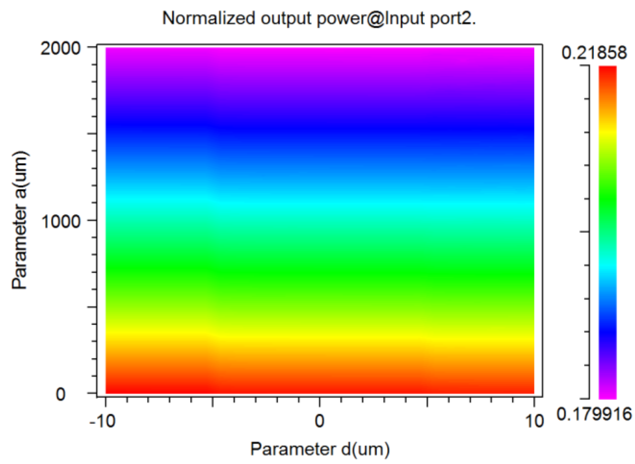

(b) Light input from port 2

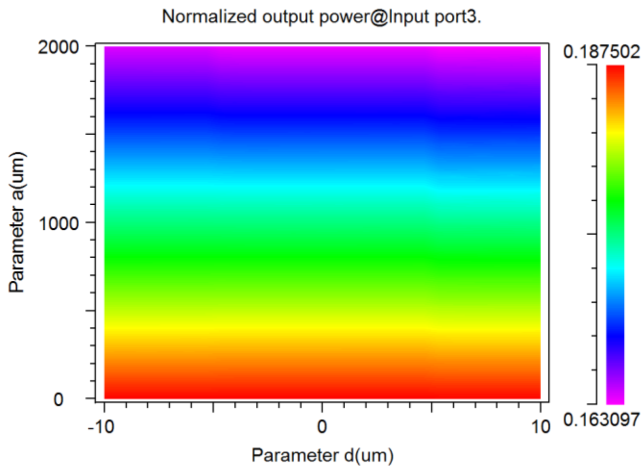

(c) Light input from port 3

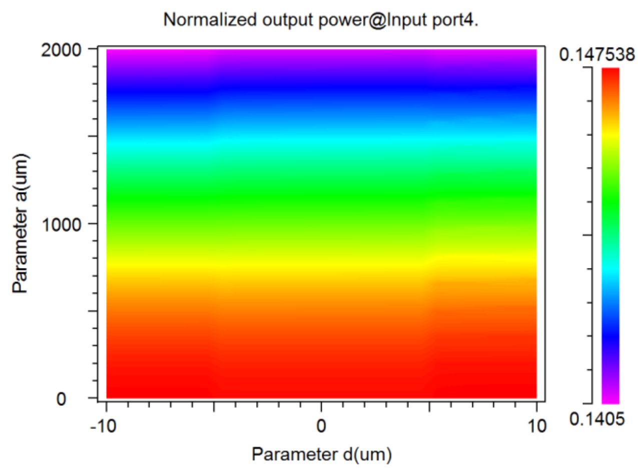

(d) Light input from port 4

*Fig. 3. Normalized output power with parameter **α** and **d** variation at four ports*

Similarly, when light inputs from port 1, larger normalized output power is the green or red part in Fig. 4(a). That is, parameter ***b*** is within 8~16 μm or 24~25 μm and best parameter ***c*** is within 10~16 μm. While light inputs from port 2, best normalized output power is the red part in Fig. 4(b). That is, best parameter ***b*** is within 8~16 μm and best parameter ***c*** is within 10~19 μm. When light inputs from port 3, best normalized output power is the red part in Fig. 4(c). That is, best parameter ***b*** is within 8~16 μm and best parameter ***c*** is within 10~18 μm. Simultaneously, while light inputs from port 4, best normalized output power is the red part in Fig. 4(d). That is, best parameter ***b*** is within 8~15 μm, best parameter ***c*** is within 10~17 μm. Because four figures have intersection parts, we set best value ***b*** =12 μm and ***c***= 15 μm.

Analogously, we set initial etch depth is 20 μm. While etching depth parameter ***i*** changes, total etch depth is (20+***i***) μm. When parameter ***i*** changes from -5 μm to 15 μm, best normalized output power is also obtained.

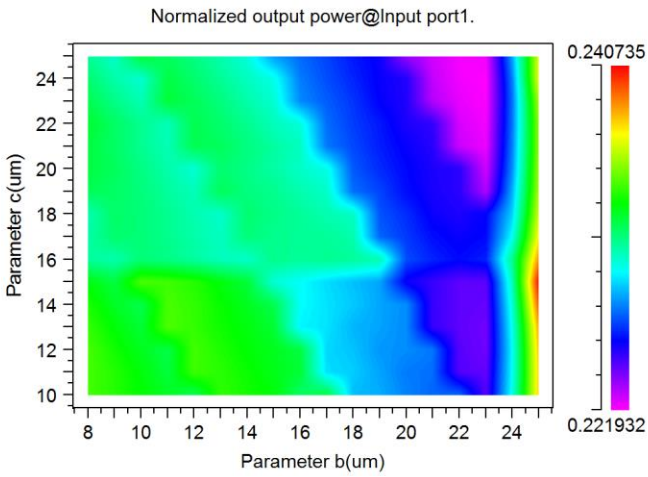

(a) Light input from port 1

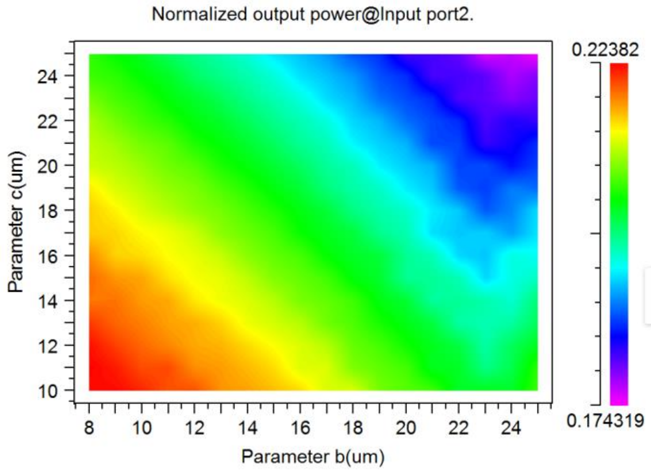

(b) Light input from port 2

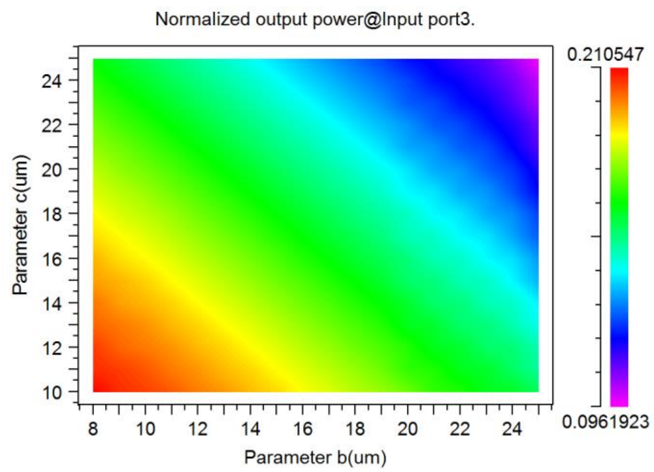

(c) Light input from port 3

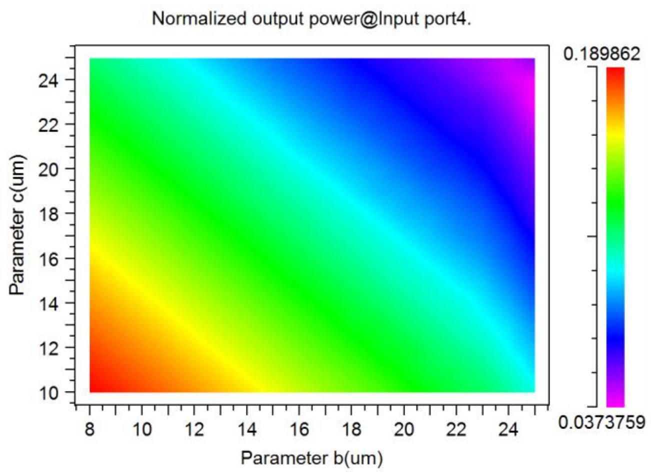

(d) Light input from port 4

Fig. 4. Normalized output power with parameter b and c variation at four ports

In Fig. 5(a), when light inputs from port 1, the parameter ***i*** ranges from -5 µm to 15 µm, normalized output power gradually increases, best normalized output power is greater than 0.258. In Fig. 3(b), when light inputs from port 2, the parameter ***i*** ranges from -5 µm to 15 µm, normalized output power gradually increases, normalized output power is also greater than 0.227. In Fig. 3(c), when light inputs from port 3, the parameter ***i*** ranges from -5 µm to 15 µm, normalized output power gradually increases, best normalized output power is greater than 0.19. In Fig. 3(d), when light inputs from port 4, the parameter ***i*** ranges from -5 µm to 15 µm, normalized output power is gradually reduced, the least normalized output power is also lower than 0.147. From above four figures, we can get the best changing range of i value, that is, best value ***i***=0～3 µm.

Analogously, while spacing of neighboring input ridge waveguides (parameter ***c***) randomly changes, best directivity can be obtained.

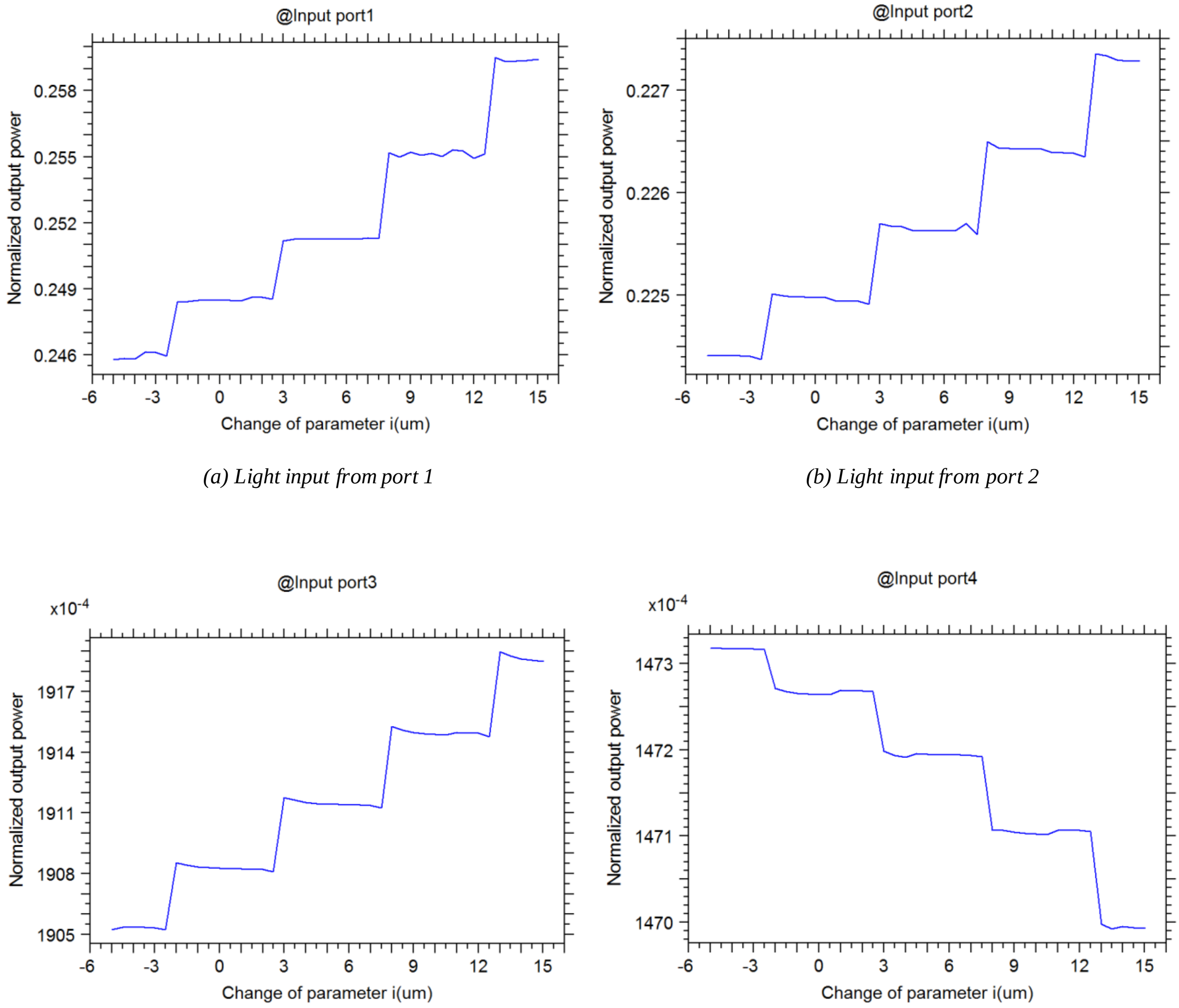

(a) Light input from port 1 *(b) Light input from port 2*

(c) Light input from port 3 *(d) Light input from port 4*

*Fig. 5. Normalized output power with parameter **i** variation at four ports*

In Fig. 6(a), when light inputs from port 1, parameter ***c*** varies over 10 µm, directivity is greater than 50 dB. In Fig. 6(b), while light inputs from port 2, parameter ***c*** varies over 10 µm, directivity is also greater than 50 dB. In Fig. 6(c), when light inputs from port 3, parameter ***c*** varies over 10 µm, directivity is still greater than 50 dB. In Fig. 6(d), while light inputs from port 4, parameter ***c*** varies over 10 µm, directivity is yet greater than 50 dB. Because four figures have intersection part, we set parameter ***c*** =15 µm for best directivity.

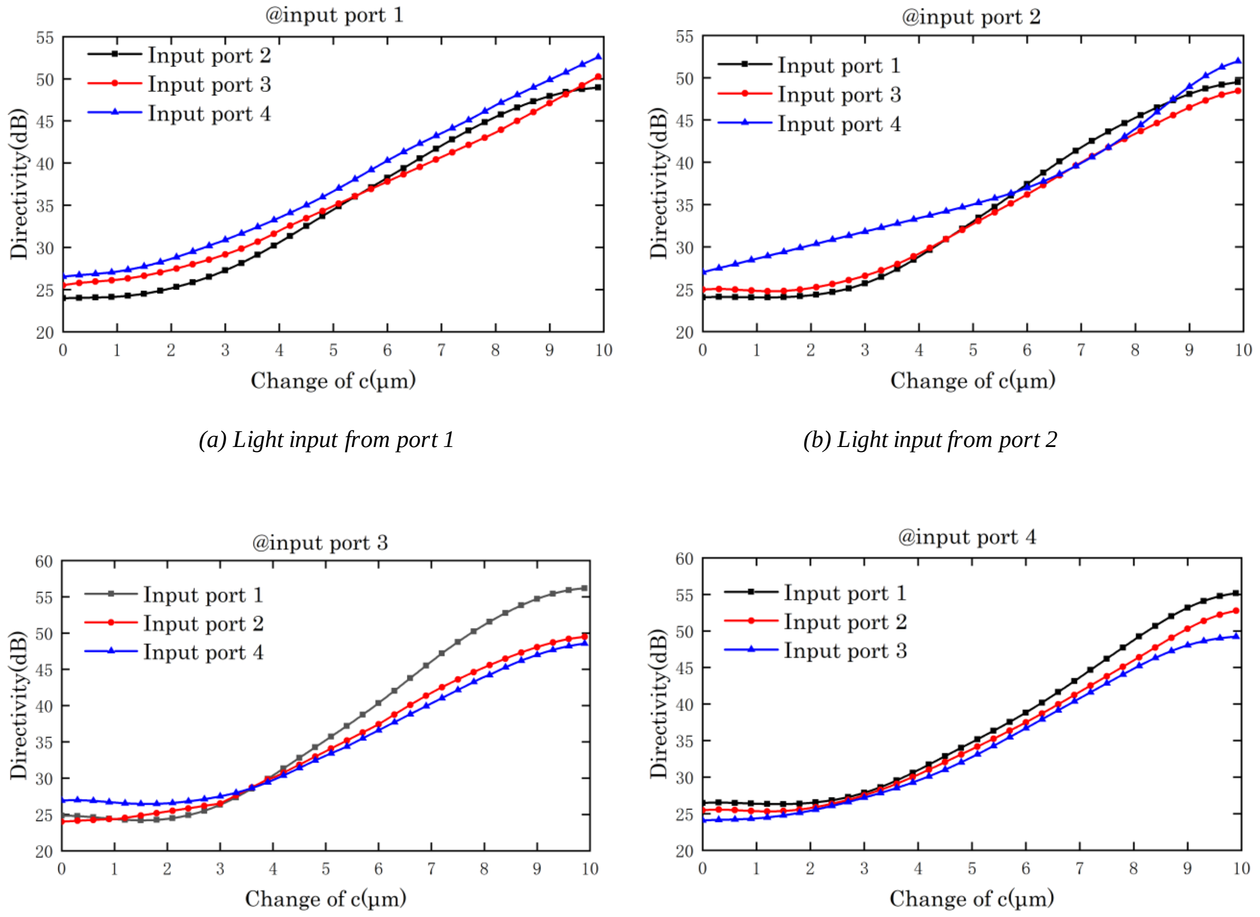

(a) Light input from port 1 *(b) Light input from port 2*

(c) Light input from port 3 *(d) Light input from port 4*

Fig. 6. Directivity with parameter c randomly variation at four input ports

3. Experimental results

In Fig. 7, the focusing lens has 20 times magnification and the numerical aperture is 0.45. The repeat frequency is 10 kHz and single pulse energy is 10 μJ in the femtosecond laser. The wavelength of femtosecond laser is 800 nm and the pulse width is 100 fs. Spot size diameter is about 6 microns. Using three-dimensional scanning etching method, scanning distance of lines is 3 micrometers, the scanning distance of inter-layers is 5 micrometers, scanning speed is 1 mm/s. In Fig. 7, after femtosecond laser passes through the energy attenuator, the power of femtosecond laser is adjusted to be slightly greater than the damage threshold of silica. Linearly polarized light is formed after passing through the half wave plate and light path is adjusted by reflector. Through a quarter wave plate, circularly polarized light is generated. After a focusing lens, a light spot with a relatively uniform power distribution is formed and focused on the surface of silica chip. The computer controls three-dimensional platform to precisely move for manufacturing silicon dioxide 8×1 MCRC by programs. The 8×1 MCRC have been fabricated in Fig. 8.

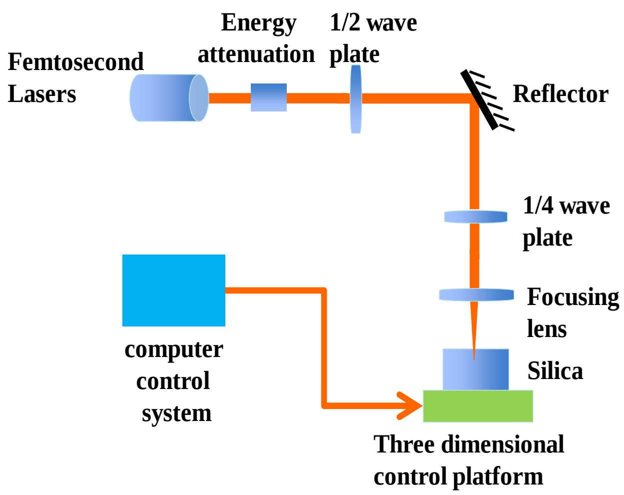

Fig. 7. Light-path diagram for manufacturing chip

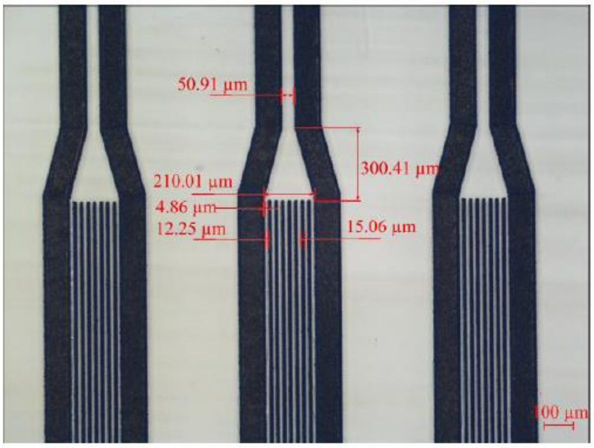

(a) *Top view of 8×1 MCRC*

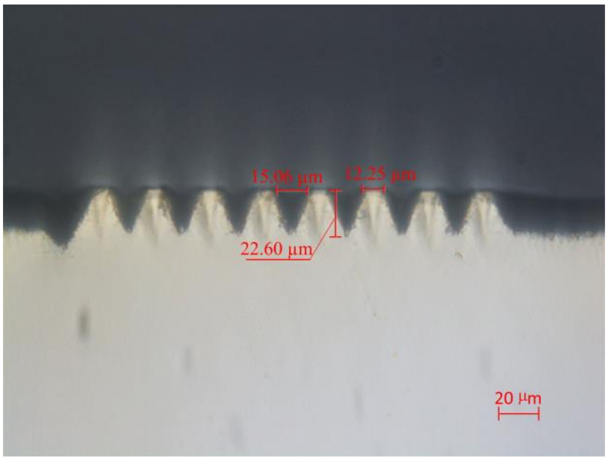

(b) *Front view of 8×1 MCRC*

Fig. 8. Test diagram of 8×1 MCRC

In Fig. 8(a), We can clearly see that width of input ridge waveguide is 12.25 µm and manufacturing error is 0.25 µm. Spacing between input ridge waveguides is 15.06 µm and design error is 0.06 µm. The width of input port of taper ridge waveguide is 210.01 µm and manufacturing error is 0.99 µm. The length of tapered ridge waveguide is 300.41 µm and manufacturing error is 0.41 µm. The width of output multimode ridge waveguide is 50.91 µm and the manufacturing error is 0.91 µm. The Spacing between straight waveguide and the edge of multimode tapered waveguide is 4.86 µm and the manufacturing error is 0.14 µm. In Fig. 8(b), we can obviously find that height of input ridge waveguide is 22.60 µm and manufacturing error is 2.60 µm. These above manufacturing error values are actually in the design error range. They have little effect on the optical transmission performance of the 8×1MCRC. So, ten mode coupling receiver chips have been fabricated. Their average insertion loss (dB), average return loss (dB), average directivity (dB), have been tested, respectively. These results are shown in Table 1.

Table 1. Average optical properties of ten MCRCs

Input port	1	2	3	4	5	6	7	8
Wavelength (nm)	1310±50 nm							
average insertion loss (dB)	11.55	11.48	12.23	12.47	11.72	11.46	12.15	12.24
average return loss (dB)	51.06	51.22	51.23	50.97	50.34	51.14	50.82	51.33
average directivity (dB)	56.76	55.94	56.13	55.86	56.27	56.04	56.38	55.87

From these experimental results, we can find that insertion loss ≤13 dB, return loss ≥50 dB, directivity >55 dB. In addition, the average bit error rate of MCRC is 1.583×10^{-10} in signal upstream for every input port by bit error tester. This manufacturing method meets design requirements.

4. Conclusions

In this paper, the 8×1 mode coupling receiver chip is designed for lossless optical splitter. Depth of core of multimode tapered waveguide is 300 µm. Length of long side in the core of multimode tapered waveguide is 211 µm. Length of short side in the core of multimode tapered waveguide is 50 µm. Width of core of inputting straight waveguide is 12 µm. Distance between core of inputting straight waveguides is 15 µm. Etch depth is 23 µm. Actually, we have manufactured ten 8×1 MCRCs. The width of input ridge waveguide is 12.25 µm. Spacing between input ridge waveguides is 15.06 µm. The width of input port of tapered ridge waveguide is 210.01 µm. The length of tapered ridge waveguide is 300.41 µm. The width of output multimode ridge waveguide is 50.91 µm. The height of input ridge waveguide is 22.60 µm. The distance between straight waveguide and edge of the multimode tapered waveguide is 4.86 µm. Manufacturing error values are within the design error range. Test results show that average insertion loss ≤13 dB, average return loss ≥50 dB, average directivity >55 dB. Average bit error rate is 1.583×10^{-10} in signal upstream for every input port. This manufacture meets the industry requirements. It is very beneficial for next-generation PONs.

Acknowledgments

This research was supported by Provincial Natural Science Foundation of Hubei (ZRMS2017001448). Hubei University of Technology Doctor Research Funding (00026). Hubei University of Technology "Advanced Manufacturing Technology and Equipment" Collaborative Innovation Center Open Research Fund (1201501). Hubei University of Technology Green Industry Technology Leading Project (CPYF2017002). Research Project of Hubei Provincial Department of Education (T201405). Research Project of Hubei Provincial Department of Education (D20181401).

References

[1] Ning Cheng, Zhenxing Liao, Frank J. Effenberger, 36th European Conference and Exhibition on Optical Communication 04 (2010).

[2] Franz Fidler, Oswald Wallner. EURASIP Journal on Wireless Communications and Networking **2008**, art. No. 20 (2008).

[3] W. Kam, Y. S. Ong, W. H. Lim, R. Zakaria, Optics and Lasers in Engineering **55**, 1 (2014).

[4] K. F. Tamrin, S. S. Zakariyah, N. A. Sheikh, Optics and Lasers in Engineering **75**, 48 (2015).

[5] A. K. Sheridan, C. B. E. Gawith, G D. Emmerson, J. A. Milton, J. S. Wilkinson, Optics Communications **242**(1–3), 109 (2004).

[6] Ying Wan, Yang Zhang, Zuosen Shi, Wenhui Xu, Zhanchen Cui, Polymer **53**(4), 967 (2012).

[7] Alejandro Muriano, K. N. Anisha Thayil, J. Pablo Salvador, Pablo Loza-Alvarez, M. Pilar Marco, Sensors and Actuators B: Chemical **174**, 394 (2012).

[8] Koen Vanmol, Salvatore Tuccio, Vivek Panapakkam, Hugo Thienpont, Jürgen Van Erps, Optics & Laser Technology **112**, 292 (2019).

[9] Yicun Yao, Chao Zhang, Sudheer Kumar Vanga, A. A. Bettiol, Feng Chen, Optical Materials **35**(12), 2257 (2013).

[10] A. A. Bettiol, S. Venugopal Rao, T. C. Sum, J. A. van Kan, F. Watt, Journal of Crystal Growth **288**(1), 209 (2006).

[11] M. De Vittorio, M. T. Todaro, T. Stomeo, R. Cingolani, E. Di Fabrizio, Microelectronic Engineering **73–74**, EX1 (2004).

[12] Jiajia Mu, Jiafang Li, Wuxia Li, Qiang Luo, Changzhi Gu, Microelectronic Engineering **110**, 307 (2013).

[13] Bin Zhang, Bingcheng Xiong, Ziqi Li, Lingqi Li, Feng Chen, Optical Materials **86**, 1 (2018).

[14] Ziqi Li, Chen Cheng, Carolina Romero, Qingming Lu, Feng Chen, Optical Materials **73**, 45 (2017).

[15] Koji Igarashi, Kyung Jun, Park, Takahiro, Tsuritani, Itsuro Morita, Byoung Yoon Kim, Optics Communications **408**, 58 (2018).

[16] Jiaxiong Li, Jiangbing Du, Lin Ma, Ming-Jun Li, Zuyuan He, Optics Communications **383**, 42 (2017).

[17] Yongqiang Hei, Li Li, Wentao Li, Xiaohui Li, Guangming Shi, Optical Fiber Technology **41**, 182 (2018).

[18] Fang Ren, Juhao Li, Zhongying Wu, Tao Hu, Zhengbin Li, Optics Communications **383**, 525 (2017).

*Corresponding author: dun.liu@hbut.edu.cn